Observed seasonal to decadal-scale responses in mesospheric water vapor

Ellis Remsberg[1]

[1]Science Directorate, NASA Langley Research Center, Hampton, VA

E. E. Remsberg, Science Directorate, Mail Stop 401B, NASA Langley Research Center, Hampton, VA 23681-2199. (e-mail: Ellis.E.Remsberg@nasa.gov)

Abstract.

The 14-yr (1991-2005) time series of mesospheric water vapor from the Halogen Occultation Experiment (HALOE) are analyzed using multiple linear regression (MLR) techniques for their seasonal and longer-period terms from 45S to 45N. The distribution of annual average water vapor shows a decrease from a maximum of 6.5 ppmv at 0.2 hPa to about 3.2 ppmv at 0.01 hPa, in accord with the effects of the photolysis of water vapor due to the Lyman-α flux. The distribution of the semi-annual cycle amplitudes is nearly hemispherically symmetric at the low latitudes, while that of the annual cycles show larger amplitudes in the northern hemisphere. The diagnosed 11-yr, or solar cycle, max minus min, water vapor values are of the order of several percent at 0.2 hPa to about 23% at 0.01 hPa. The solar cycle terms have larger values in the northern than in the southern hemisphere, particularly in the middle mesosphere, and the associated linear trend terms are anomalously large in the same region. Those anomalies are due, at least in part, to the fact that the amplitudes of the seasonal cycles were varying at northern mid latitudes during 1991-2005, while the corresponding seasonal terms of the MLR model do not allow for that possibility. Although the 11-yr variation in water vapor is essentially hemispherically-symmetric and anti-phased with the solar cycle flux near 0.01 hPa, the concurrent temperature variations produce slightly colder conditions at the northern high latitudes at solar minimum. It is concluded that this temperature difference is most likely the reason for the greater occurrence of polar mesospheric clouds at the northern versus the southern high latitudes at solar minimum during the HALOE time period.

1. Background and Objectives

Water vapor (H_2O) in the low to middle mesosphere is determined by its so-called "entry level" value to the stratosphere from the tropical upper troposphere plus the effects of the oxidation of methane (CH_4) to H_2O in the upper stratosphere. That conversion of CH_4 to H_2O is essentially complete for air reaching the middle mesosphere. Water vapor and its component radicals also interact chemically with odd oxygen in the mesosphere. The distribution of H_2O in the middle and upper mesosphere is determined by the effects of global-scale, net transport processes and by photolysis from Lyman-alpha (Ly-α) radiation that is most efficient near the mesopause. The largest periodic variations of H_2O in the upper mesosphere are found at the higher latitudes and on both seasonal and 11-yr (or solar cycle) time scales. Thus, the observed variations of H_2O can be a useful diagnostic of the performance of radiative-chemical-transport models and of global change in the mesosphere [*Brasseur and Solomon,* 1984; *Laštovička et al.,* 2008].

Currently, only a few multiyear datasets are available for characterizing the large-scale variations of water vapor in the mesosphere. In particular, H_2O profiles were obtained with a vertical resolution of about 2.5 km from cloud tops to just above the 0.01-hPa level for more than one complete solar cycle (1991-2005) by the Halogen Occultation Experiment (HALOE) of the Upper Atmosphere Research Satellite (UARS) [*Russell et al.,* 1993; *Harries et al.,* 1996; *Kley et al.,* 2000]. Individual retrieved H_2O mixing ratio profiles appear rather noisy (or oscillatory with altitude) in the mesosphere, due to the non-linear relationship between the retrieved H_2O and the small changes of the observed 6.6-μm limb transmission values. Therefore, this study analyzes time series of points obtained by averaging mixing ratio profiles for each of the HALOE sunset

58 (SS) and sunrise (SR) orbital crossing occurrences of selected latitude zones. In order to obtain
59 reasonable zonal mean estimates for a latitude crossing, the profiles are binned according to 20
60 degree-wide latitude zones. A minimum of 5 profiles is required for a bin-average, although
61 most of the averages are derived from many more profiles. These criteria are providing time
62 series points that are much less noisy and are representative of zonal means because the large-
63 scale longitudinal gradients of H_2O are weak in the mesosphere at low and middle latitudes.

64

65 Section 2 describes briefly the multiple linear regression (MLR) model analysis approach that is
66 used to obtain the seasonal and longer-term variations of HALOE Version 19 (V19) H_2O versus
67 latitude and for pressure-altitudes from 0.2 to 0.01 hPa. It also provides the latitude versus
68 pressure distributions of the amplitudes of the semi-annual and annual terms from the regression
69 models. Section 3 shows results for the 11-yr or the solar cycle (SC-like) terms and relates the
70 distribution of their "max minus min" H_2O values with those from model simulations reported in
71 the literature. It also contains findings for the concurrently analyzed, linear trend terms and of
72 the potentially confounding effects for the determination of their SC-like responses. Section 4
73 discusses the SC-like variations in temperature and in H_2O plus their relation to the occurrences
74 of polar mesospheric clouds (PMC) near 0.01 hPa. Section 5 summarizes the findings.

75

76 **2. Analysis Procedure and the Seasonal and QBO-like Variations**

77 *Remsberg* [2008a, his Figure 1] showed that the time series of tangent point measurement
78 locations for the HALOE SR and SS events of 2001, for example, are representative of each of
79 the seasons and for both hemispheres, at least Equatorward of about 55 degrees of latitude.

80 Conversely, the very high latitudes were not sampled at all during winter, due to the orbital
81 inclination of UARS and of the Earth with respect to the Sun. Mesospheric H_2O attains its
82 minimum values during winter at high latitudes, which means that the amplitude of its annual
83 cycle may be significantly underestimated from the HALOE data in those regions of the upper
84 mesosphere. It was also noted by *McHugh et al.* [2003] that a PMC feature in the measurement
85 line-of-sight can contaminate the retrieved H_2O profile significantly. Time series of HALOE
86 H_2O data are not considered for analysis at the higher latitudes for these reasons.

87

88 The MLR analysis approach of the present study follows that given in *Remsberg* [2008a] and is
89 described briefly here. Zonal, bin-averages of the V19 SS and then the SR profiles are obtained
90 for ten, 20-degree wide latitude zones from 45S to 45N and for 9 pressure levels from 0.2 hPa (or
91 near 60 km) to 0.01 hPa (or near 80 km). Each of the 90 time series of the set of SS plus SR H_2O
92 is analyzed by MLR techniques to obtain their annual oscillation (AO) and semi-annual
93 oscillation (SAO) terms, any weak quasi-biennial oscillation (QBO)-like and sub-biennial
94 (interannual or IA) terms, their decadal-scale (11-yr) terms, and linear trend terms. The sub-
95 biennial term occurs as a result of interactions between the AO and QBO terms, and it has a
96 period of about 21 months. For a given latitude bin and pressure-altitude the amplitudes and
97 phases of the periodic terms, including the QBO and 11-yr terms, are based on a fitting with a set
98 of predictors that are simply harmonics of specific periods. This approach differs from the more
99 common practice of fitting to a proxy for an underlying physical process, such as the f10.7-cm
100 flux for the SC and a couple of tropical wind indices for the QBO term (e.g., *Randel et al.*, 2000;
101 *Wallace et al.,* 1993). On the other hand, the present approach is particularly useful for

identifying interannual responses in the mesosphere and for determining whether the primary decadal-scale response of H_2O is truly anti-phased with the SC uv-flux forcing.

It is easy to confound the effects of SC and trend terms for the time series, especially when adjacent zonal mean points are correlated. Those effects are accounted for to first order by conducting a two-step process with the MLR model in the manner of *Tiao et al.* [1990] and *Remsberg* [2008a]. Initially, the set of relevant model terms are fit to the H_2O time series, and a weak positive, lag-1 autoregression (AR1) coefficient is obtained from the time series of the noise residuals. Then, the model terms are transformed to account for the AR1 coefficient, and the data time series are refit to obtain the coefficients for the final MLR terms.

At this point it is noted that the 14-yr time series consist of alternating SR and SS points and that there are slight differences between the means of the SR and SS H_2O values for several extended periods of the dataset. Those differences are due to small biases from the FOV lockdown of the HALOE instrument in its SR transmission profiles. The effect is evident as an exaggerated vertical oscillation in the retrieved SR H_2O profile near 0.1 hPa—the H_2O values are too small just below and too large just above that pressure level. The incorrect lockdown for those SR scans leads to weakly negative AR1 coefficients that are accommodated by the transformed terms of the final MLR model for the combined (SR plus SS) HALOE H_2O time series.

Figure 1 is an example time series of HALOE V19 H_2O at 35N and 0.015 hPa (near 75 km). The solid and open points are the bin-averaged SS and SR values, respectively, for HALOE tangent-point measurements made at 35±10N throughout the years. The oscillating curve is the MLR model fit to the points, and it is composed of constant (Const), AO, SAO, QBO (853-dy or 28 mo), IA (640-dy or 21-mo), 11-yr (or SC-like), and linear (Lin) trend terms. There is a clear annual cycle in the data at this latitude and level. The straight line in Figure 1 is just the sum of the Const and Lin terms. Figure 2 is the time series of the data minus model residuals (in ppmv) from Figure 1. No apparent periodic structure is remaining in those residuals—an important test for the acceptance of the final MLR model.

The HALOE H_2O data time series of Figure 1 exhibits a weak, near-biennial variation; the amplitude of the associated, model QBO (28-mo) term is discussed later in this section. There are also clear relative minima at about 1991 and 2002, in accord with the estimated times for the maxima of the Ly-α photolysis flux of the 11-yr solar cycle. Such a direct response is expected for the upper mesosphere. The response to Ly-α is much weaker in the middle mesosphere and is most likely mixed with the larger H_2O responses of the higher altitudes and latitudes as a result of its annually-averaged, net circulation. In order to assess the prospect of a delayed, SC-like response for the H_2O of the middle mesosphere, a simple sinusoid of 11-yr period was used to fit the data at all altitudes and latitudes. The amplitudes of the 11-yr terms were determined, but then the phases were checked to see how well the 11-yr H_2O maxima coincided with the estimated minima for a Ly-α or other solar cycle (SC) flux proxy. Findings for the 11-yr terms are presented and discussed in Section 3.

144

145 Figures 3-5 show the latitude versus pressure cross sections of (a) the constant term (in ppmv),
146 (b) the amplitude of the SAO term (in %), and (c) the amplitude of the AO term (in %),
147 respectively. Since HALOE samples a latitude zone infrequently, one must combine the
148 constant term, seasonal amplitudes, and their phases, in order to generate an H_2O distribution for
149 comparisons with models at a specific time of the year, for example in January. *Jackson et al.*
150 [1998] showed and discussed these terms for the mesosphere from the first 5 years of the
151 HALOE data, and the results of this section are compared with them briefly. Figure 3 is the
152 distribution of the constant terms, i.e., their 14-yr, annual average H_2O mixing ratios. Those
153 values decrease from a maximum of about 6.5 ppmv in the mid-mesosphere to 3.2 ppmv near
154 0.01 hPa. Estimates of total bias error for HALOE zonal mean H_2O are of order 10% in the
155 mesosphere [*Harries et al.,* 1996]. Comparisons with other satellite data indicate that the
156 HALOE values may be, in fact, too low but by no more than 12% in the same altitude region
157 [*Lambert et al.,* 2007; *Milz et al.,* 2009]. The relative variations of HALOE H_2O with altitude
158 and latitude are likely more accurate because the primary systematic errors do not depend on
159 atmospheric state. The decreasing values of H_2O with altitude are due largely to the effects of
160 Ly-α photolysis. Their decrease toward higher latitudes is indicative of the descent of air at polar
161 winter latitudes. There is also a slight hemispheric asymmetry for the northern versus the
162 southern latitudes for this distribution.

163

164 Figure 4 is the distribution of the SAO amplitudes, which have their greatest percentage values
165 (or order 20%) near 0.01 hPa. This distribution agrees well with the observations of the Sub-

166 Millimetre Radiometer (SMR) instrument of the ODIN satellite [*Lossow et al.*, 2008], even near
167 0.01 hPa, where the HALOE H_2O profiles are close to their signal-to-noise limit. The HALOE
168 SAO amplitudes occur nearly symmetric about the Equator and with their minimum values in the
169 subtropics. The distribution of the phases of the SAO maxima for their first cycles is shown in
170 Table 1 (in days from January 1) and is also nearly hemispherically-symmetric. A steady
171 descent is indicated for the SAO from the upper to the middle mesosphere at the low latitudes
172 (15S to 15N), in accord with the SAO phase observations and forcings for other atmospheric
173 parameters [*Garcia et al.*, 1997]. At the middle latitudes the descent of the SAO is also
174 apparent in the southern hemisphere, while it is variable or nearly stationary with altitude in the
175 northern hemisphere.

176

177 Figure 5 is the distribution of the amplitudes of the annual cycle (AO) terms; amplitudes exceed
178 30% at the high altitudes and latitudes. The hemispheric asymmetry of this term is quite striking
179 and is responsible for the observed hemispheric asymmetry in the annual average mixing ratios
180 of Figure 3. Minimum amplitudes occur along a vertical axis centered near 15S, and this finding
181 agrees very well with the SMR observations of *Lossow et al.* [2008, see their Figure 8]. Similar
182 plots in *Jackson et al.* [1998] show that this vertical axis is nearer to 5S. On the other hand, the
183 AO amplitudes in Figure 5 are approximately the same at 45S and 45N at the 0.2-hPa level. The
184 generally smaller AO amplitudes of the southern hemisphere may be due, in small part, to the
185 fact that the Earth-Sun distance is at a minimum and the associated Ly-α flux at a maximum in
186 SH summer, which would slightly offset the tendency of the summer upwelling to increase H_2O.
187 However, this circumstance cannot explain the axis of minimum amplitudes at 15S.

188

189 Table 2 shows the time of occurrence of the AO maximum in H_2O in days past January 1. Those
190 phases are anti-symmetric between the two hemispheres (but seasonally symmetric), especially
191 at the middle latitudes. Phase propagation is more complicated in the subtropics, however. For
192 example, at the 0.05-hPa level the AO phase at 15N is very similar to that of northern middle
193 latitudes, while the AO phase at 15S is one-quarter cycle out-of-phase with that at 35-45S.
194 Clearly, the seasonal cycle in the NH versus the SH is projecting differently onto the 12-mo and
195 6-mo harmonics of the MLR fit, especially for the subtropics. Those two terms have significant
196 amplitudes at 15N and 0.05 hPa as indicated in Figure 6, while the structure of the points in the
197 corresponding time series at 15S is much weaker (not shown). Most likely the characters of
198 both the AO and the SAO in the middle mesosphere are affected by planetary Rossby waves
199 [*Dunkerton and Delisi*, 1985] and/or gravity waves [*Sato et al.*, 2009], which are
200 hemispherically-asymmetric in their occurrence.

201

202 Figure 7 is the distribution of the amplitudes of the QBO-like terms. Largest amplitudes occur at
203 middle latitudes at about 0.03 hPa, and another maximum occurs in the tropical upper
204 mesosphere. In fact, the distribution in Figure 7 is very similar to that of the QBO terms for the
205 HALOE temperature data in *Remsberg* [2008b], indicating that the interannual variability of H_2O
206 is primarily due to transport processes. The QBO amplitudes are somewhat larger in the
207 northern than in the southern hemisphere subtropics, and the minimum values occur at about
208 15S. These differences may indicate that the wave forcings associated with at least one phase of

209 the QBO cycle are interacting with the SAO forcings of the northern subtropics more effectively
210 [*Garcia et al.,* 1997].

211

212 At this point it is noted that the MLR analyses herein were conducted independently for each of
213 the 90 HALOE H_2O time series. Therefore, an important measure of the quality of the results in
214 Figures 3-5 and 7 is the spatial coherence of their patterns with altitude and latitude. Uncertainty
215 for the coefficients of the terms from the MLR fit to the data is of the order of 0.20 ppmv (2-σ),
216 which is small compared with the amplitudes of the seasonal terms. Distributions for the QBO
217 and IA terms are not very significant because their amplitudes are less than 0.22 ppmv (4%)
218 everywhere. One should also be aware that the estimates of uncertainty assume that the various
219 terms of the MLR models are orthogonal to each other. That requirement is not met for the 11-yr
220 and linear trend terms of the 14-yr HALOE time series.

221

222 **3. Decadal-scale Responses in Water Vapor**

223 Early analyses of the mesospheric response of HALOE water vapor to the variations of solar Ly-
224 α were provided by *Randel et al.* [2000] and *Chandra et al.* [1997]. *Randel et al.* [2000]
225 reported a "max minus min" variation of 21% for the period 1992-99, while *Chandra et al.*
226 [1997] reported an increase of 41% from January 1992 to December 1995, both at 0.01 hPa. Part
227 of their differences may be traceable to the HALOE version 19 dataset used by *Randel et al.*
228 [2000] versus the version 18 data employed by *Chandra et al.* [1997]. Their findings may also
229 have been affected by the underlying trends for H_2O that are increasing in the mesosphere
230 through the 1990s; the trends are more nearly flat thereafter [*Nedoluha et al.,* 2009].

As noted in Section 2, the approach to the SC analyses herein has been to simply fit the HALOE water vapor time series with a sinusoid of 11-yr period and then to check its phase to see how closely it conforms to an estimate of the variations of the direct Ly-α flux. Since H_2O is photolyzed most effectively at solar maximum, its 11-yr responses are plotted for solar "max minus min" (as a percent of its average value) and are therefore negative. Figure 8 is a contour plot of that full change in H_2O (i.e., twice its amplitude), which varies from about 4% near 0.2 hPa to about 23% at 0.01 hPa, the latter value agreeing most closely with the values of *Randel et al*. [2000] and *Nedoluha et al.* [2009]. Values of 4% are just significant at the 2-σ level; the greater percentage values are considered highly significant.

Figure 9 is the phase of the maximum of the 11-yr H_2O response (in years past January 1991 or 2002). The dashed contour denotes the 5.5-yr value or July 1996, the approximate time of solar flux minimum (or water vapor maximum). In the middle mesosphere the water vapor maximum is lagging solar flux minimum by about 1 year at middle latitudes and by nearly 2 years in the tropics. However, the phases of those weak amplitude terms are just barely significant, and they are the terms that are most likely to be confounded with the associated linear trend terms (see further discussion in the last paragraph of this section).

Figure 10 is the plot of the so-called SC-like H_2O responses. They were obtained by adjusting the 11-yr responses of Figure 8 by the fact that they were not quite in-phase with the Ly-α flux

252 forcing—i.e., an adjustment by the cos [(t-5.5)/11], where t is the time of the 11-yr water vapor
253 maximum from Figure 9. In effect, this adjustment accounts for the possibility that there are
254 other decadal-scale forcings for the H_2O that were not considered in the MLR model. There is
255 little change for the H_2O responses between Figures 10 and 8 for the upper mesosphere. Those
256 max minus min H_2O percentage variations are opposite in sign but very similar in magnitude to
257 the observed 11-yr changes in the Lyman-α flux [*Tobiska et al.,* 1997; *Deland et al.,* 2004]. The
258 adjusted, max minus min H_2O variations are altered the most for the tropical middle mesosphere
259 and are now no larger than about 2%. The 11-yr and the SC-like responses are nearly symmetric
260 about the Equator in the uppermost mesosphere. However, the diagnosed responses at middle
261 latitudes are about twice as large in the northern as in the southern hemisphere, indicating a
262 potentially confounding influence from the trend terms.

263

264 Model H_2O solar cycle responses agree well with the HALOE findings in the uppermost
265 mesosphere, once an accommodation is made for the fact that the percentage responses for many
266 of the models are referenced to their 11-yr H_2O minimum values rather than to the response
267 average, as in Figures 8 and/or 10 [e.g., *Garcia et al.,* 1984; *Huang and Brasseur,* 1993; and
268 *Schmidt et al.,* 2006]. The SC-like response profile from Figure 10 at 20N also agrees well with
269 that from the Water Vapor Millimeter-wave Spectrometer (WVMS) instrument at Mauna Loa for
270 the concurrent period of the HALOE data [*Nedoluha et al.,* 2009].

271

272 The MLR models include linear trend terms, and Figure 11 is their distribution (in %/decade).
273 Values vary from 12 (or 1.2%/yr) at 40N and 8 (or 0.8%/yr) at 40S to nearly no change at the
274 Equator. Such large values for the middle latitudes of the mesosphere are unphysical compared
275 with the model simulations of about 4%/decade, due primarily to the trends from the oxidized
276 methane [*Garcia et al.*, 2007]. It is also noted that no significant changes in the HALOE
277 instrument have been found that might be contributing to these observed H_2O trends and, in
278 particular, their variations with latitude in Figure 11 [*Gordley et al.*, 2009].

279

280 The distribution of trends in the tropics to subtropics of Figure 11 is qualitatively consistent with
281 the H_2O and CH_4 trends of the stratosphere of several years earlier. For example, *Randel et al.*
282 [2006] reported H_2O increases of order 1%/yr in the lower stratosphere from HALOE data for
283 the decade of the 1990s, followed by a decreasing to no trend after 2001. *Scherer et al.* [2008]
284 found H_2O trends from balloon-borne, frostpoint measurements at Boulder of -0.2 to 1.0%/yr for
285 altitudes from 14 to 25 km for the same period with a clear change of trend in 2000/2001.
286 Trends in tropospheric CH_4 were variable and generally positive (~0.3%/yr) through the 1990s,
287 but also slowed to near zero thereafter [*Dlugokencky et al.*, 2009]. Correspondingly, the
288 observed positive trends of CH_4 for the lower stratosphere slowed to about zero during the
289 HALOE period [*Rohs et al.*, 2006]. It is reasonable to assume from the age-of-air characteristics
290 for the H_2O and CH_4 entering the lower tropical stratosphere that their trends will be retained (at
291 least to some extent) as that air is transported upward over a period of several years to near the
292 stratopause by the Brewer/Dobson circulation [*Shepherd*, 2007]. However, because the
293 exchange of air between low and high latitudes is much more efficient in the mesosphere, the

294 diagnosed HALOE trends of the middle latitudes cannot be due to the changing stratospheric
295 source gases.

296

297 The character of the MLR fit at northern middle latitudes is examined further in Figure 12 for
298 35N and the 0.05-hPa level. A closer look at the annual cycle variations in the data reveals that
299 they are smaller than those from the MLR fit during 1995-97, while they are clearly larger in the
300 data from about 2000-03. In other words, the amplitudes of the seasonal cycles in the H_2O data
301 are varying over the 14-yr time period of HALOE. Thus, the residuals that are obtained after the
302 time series data are de-seasonalized will contain some longer-period structures that are being
303 accounted for by the interannual, 11-yr, and linear trend terms of the MLR model. The
304 constraint of the seasonal-cycle fit is contributing to the anomalous character of the diagnosed
305 11-yr and trend terms.

306

307 It is postulated that the rather marked difference for the 11-yr and trend terms of the two
308 hemispheres is also an indicator of the differences for the seasonal exchanges of air between the
309 middle and high latitudes. During winter there is descent of air having low H_2O values in the
310 polar vortex. The degree to which that air is transported and/or mixed to lower latitudes depends
311 on the extent to which the vortex remains intact through the winter/spring period, and generally
312 there is more wintertime wave activity propagating to the mesosphere from below in the northern
313 hemisphere [*Sato et al.*, 2009]. Northern hemisphere, mid-winter warming events in the upper
314 stratosphere are accompanied by a cooling in the mesosphere, a weakening or breakdown of the

polar night jet, and an enhanced meridional transport and mixing of the air. Such mid-winter events are rarely found in the southern hemisphere. *Pawson and Naujokat* [1999] reported that there was very little mid-winter wave activity at NH high latitudes during most of the 1990s, while *Manney et al.* [2005] found such activity to be prevalent for 6 of the next 7 years. Since H_2O has a significant meridional gradient in the middle mesosphere at the mid latitudes (Figure 1), it is reasonable to conclude that the degree to which the seasonal cycles of the model do not match the data in Figure 12 is an important indicator of the response of the transport to those events. Such activity may bear little relation to the solar cycle forcing, although there is no way to know for sure based on this rather short, 14-yr HALOE dataset.

Observations of increasing lower stratospheric H_2O trends up to 2001, followed by decreasing trends thereafter, strongly suggest that 14 years is much too short a time for an analysis of its trends. The findings herein from the HALOE dataset also support that contention for the mesosphere. As *Garcia et al.* [2007] argued, one may need 30-40 years of data before one can estimate a true secular trend in water vapor for the middle atmosphere.

4. Implications of the Solar Cycle Responses in H_2O

There have been a number of observational and model studies of the effects of water vapor in the upper mesosphere and its relation to the occurrence of PMCs near 0.01 hPa [e.g., *Shettle et al.*, 2009; *Sonnemann and Grygalashvyly*, 2005]. Although the analyses of the HALOE water vapor responses herein do not quite extend to the high latitudes of the PMCs, Figure 5 indicates that the

337 AO term has larger percentage responses in the northern than in the southern hemisphere for that
338 region of the upper mesosphere. Maximum H_2O mixing ratios occur in the summer at high
339 latitudes. Recall that Figure 9 indicates that PMCs should also occur most frequently at solar
340 minimum, when H_2O values are at their maximum. On the other hand, Figure 10 shows that the
341 percentage changes for the SC-like responses of H_2O are nearly identical for the two
342 hemispheres near 0.01 hPa, indicating that there should be no hemispheric difference in the SC-
343 like occurrence of PMCs due to water vapor.

344

345 The observed greater seasonal occurrence of PMCs in the northern versus the southern
346 hemisphere would be aided by slightly colder temperatures near the summer polar mesopause of
347 the northern hemisphere [*Wrotny and Russell*, 2006; *Hervig and Siskind;* 2006]. Figure 13 is the
348 plot of the HALOE AO temperature amplitudes for 10-degree wide latitude bins from 60S to
349 60N adapted from *Remsberg* [2007]. Note that although the seasonal sampling from HALOE is
350 barely adequate at the higher latitudes, signal-to-noise values in the mesosphere are much larger
351 for the temperature than for the H_2O measurements. Therefore, the MLR analyses were
352 extended to higher latitudes for temperature, and it was found that its AO amplitudes agree
353 closely with those from the earlier satellite temperature climatology of *Barnett et al.* [1985].

354

355 Figure 13 shows that the seasonal temperature variations of the upper mesosphere extend farther
356 into the subtropics for the northern hemisphere—an indication of the associated effects of the net
357 transport for the two hemispheres. Note also that the AO temperature amplitudes at the high

358 latitudes are larger by up to 4 K in the southern than in the northern hemisphere, potentially
359 leading to formation of more PMC in southern hemisphere summer. But when those AO
360 temperature variations are referenced to the annually-averaged temperatures of Figure 14 that are
361 colder by up to 5 K near 0.01 hPa in the northern versus the southern high latitudes, it is the high
362 latitudes of the northern hemisphere that are actually favored slightly for PMC formation. Thus,
363 it should be clear that if one wants to reconstruct the actual temperature from the MLR fit, one
364 needs to know the constant term and resolve both the annual and semiannual harmonics from the
365 HALOE data time series. Although the seasonal sampling for the HALOE H_2O measurements
366 was marginal at the high latitudes where PMCs occur, the combination of slightly colder
367 temperatures plus slightly larger H_2O mixing ratios at the nearby latitudes favors the formation
368 of PMC at the northern high latitudes in summer, in accord with earlier findings [*Wrotny and*
369 *Russell*, 2006; *Hervig and Siskind*, 2006].

370

371 *Remsberg* [2008b] found that the HALOE temperatures are also colder at solar minimum than at
372 solar maximum at the higher latitudes near 0.01 hPa. In other words, when the SC-like H_2O
373 mixing ratios are at their maximum, the temperatures are coldest. Furthermore, the SC-like, max
374 minus min, temperature responses (though small) are about a factor of 2 greater at the northern
375 than at the southern high latitudes of the upper mesosphere, as shown in Figure 15. Therefore, it
376 is tentatively concluded that the occurrence of PMCs is significantly greater at solar minimum in
377 the northern hemisphere than in the southern hemisphere due to the temperature differences, in
378 accord with the earlier estimates of *Hervig and Siskind* [2006], *Siskind et al.* [2005] and *Wrotny*
379 *and Russell* [2006]. Even so, it may be that this finding is unique to the HALOE time period, as

opposed to being a regular occurrence [e.g., *Luebken et al.*, 2009]; longer time series are needed to verify that prospect.

Marsh et al. [2003] analyzed HALOE ozone for its response to HOx (and H_2O) in the upper mesosphere and reported that only its SS (not SR) ozone was sensitive to those changes. They also found significant decreases in HALOE ozone associated with a nearly linear increase of about 1%/yr in the HALOE H_2O, at least for the period of 1991-2001. However, the results of Figure 11 indicate much weaker H_2O trends at most latitudes based on the full 14-yr HALOE dataset. It is very likely that the associated ozone trends are smaller, too. The overall response of mesospheric ozone to the H_2O from HALOE should be reanalyzed and compared with the model simulations of the SC-like responses of ozone [e.g., *Schmidt et al.*, 2006; *Marsh et al.*, 2007; *Tsutsui et al.*, 2009]. Still, the direct effects of the solar cycle forcing for ozone are much smaller than for H_2O in the upper mesosphere. Thus, the attribution of trends in ozone to any long-term changes in the H_2O is affected by the precision of the ozone and requires further study.

5. Summary Findings

The HALOE measurements were obtained with a sampling frequency that is adequate for resolving the seasonal and longer-term variations at low and middle latitudes. Its 14-yr (1991-2005) time series of H_2O were analyzed for those variations in the middle and upper mesosphere. The distribution of the annual average H_2O shows a decrease from a maximum of about 6.5 ppmv in the mid-mesosphere to 3.2 ppmv near 0.01 hPa, in accord with the effects of the photolysis of H_2O due to the Ly-α flux. Although SAO cycle amplitudes are hemispherically-

402 symmetric at low latitudes, AO cycle amplitudes are clearly larger in the northern than the
403 southern hemisphere. It is presumed that this hemispheric asymmetry is reflective of a stronger
404 net circulation for the northern latitudes, particularly during winter and springtime.

405

406 The response of a periodic, 11-yr term is essentially anti-phased with that of the solar cycle flux
407 in the upper mesosphere. Its "max minus min" H_2O responses vary from about 4% at 0.2 hPa to
408 about 23% at 0.01 hPa; they are nearly hemispherically-symmetric in the uppermost mesosphere.
409 At 20N the profile of the solar cycle (or SC-like) H_2O response from HALOE is in good
410 agreement with the microwave measurements of *Nedoluha et al.* [2009] and with numerical
411 model simulations generally. The 11-yr response in the mid-mesosphere is nearly anti-phased,
412 lagging that of the solar cycle flux by no more than 1 to 2 years; the response is asymmetric
413 between the northern and southern hemispheres, however. The associated linear trend terms in
414 the mid-mesosphere agree with model estimates at low latitudes, but are too large at the middle
415 latitudes of the northern hemisphere. It was found that the observed seasonal cycle in H_2O had
416 varying amplitude over that 14-yr period that was not accounted for by the AO terms of the MLR
417 model. The accompanying, de-seasonalized residuals led to anomalous results for the 11-yr and
418 trend terms in the northern hemisphere, as a result. Those variations of the observed seasonal
419 cycle amplitudes are considered an indicator of changes in the meridional transport and mixing
420 due to the wave forcing from below, although it is unclear whether there is any association with
421 the solar cycle itself. The distribution of SC-like and trend terms may be unique to the 1991-
422 2005 timeframe; data over several complete solar cycles are needed in order to know for sure.

Taken together, these analyzed, seasonal and decadal-scale H_2O variations may be useful diagnostics for assessing the validity of model transport in the mesosphere.

The combination of high H_2O and low temperature supports a higher frequency of occurrence of PMCs at high latitudes of the upper mesosphere during the summer. Although the SC-like variations in the HALOE H_2O are nearly hemispherically-symmetric in the upper mesosphere, the concurrent variations in temperature are not. Temperatures are coldest at the higher latitudes of the northern hemisphere in summer and at solar minimum. It is concluded that these conditions are likely the primary reason for a greater occurrence of PMCs in the northern versus the southern hemisphere high latitudes at solar minimum during the HALOE time period.

Acknowledgements. The author recognizes Jim Russell III, HALOE Principal Investigator, the HALOE Science Team, and the many members of the HALOE Project for producing and characterizing the high quality HALOE dataset. He also acknowledges helpful discussions with his colleague, Murali Natarajan, with regard to numerical models of the effects of a solar cycle forcing on mesospheric water vapor. The author has benefitted particularly from the insight and constructive comments of the reviewers of his manuscript. Initial findings from this work were presented at the AMS Middle Atmosphere Meeting, in Stowe, Vermont, in June 2009. Jack Kaye of NASA Headquarters provided support for this work within his Solar Occultation Satellite Science Team (SOSST) study activity.

444 **References**

445 Barnett, J. J., M. Corney, and K. Labitzke (1985), Annual and semiannual cycles based on the
446 middle atmosphere reference model in Section 2.2, in *Handbook for Middle Atmosphere*
447 *Program (MAP)*, vol. 16, edited by K. Labitzke, J. J. Barnett, and B. Edwards, pp. 175-180, Sci.
448 Comm. on Sol. Terr. Phys. Secr., Univ. of Ill., Urbana, IL.

449

450 Brasseur, G., and S. Solomon (1984), *Aeronomy of the middle atmosphere*, 441 pp., D. Reidel
451 Publ. Co., Dordrecht, Holland.

452

453 Chandra, S., C. H. Jackman, E. L. Fleming, and J. M. Russell III (1997), The seasonal and long
454 term changes in mesospheric water vapor, *Geophys. Res. Lett.*, *24*, 639-642.

455

456 Deland, M. T., L. E. Floyd, G. J. Rottman, and J. M. Pap (2004), Status of UARS solar UV
457 irradiance data, *Adv. Space Res.*, *34*, 243-250.

458

459 Dlugokencky, E. J., et al. (2009), Observational constraints on recent increases in the
460 atmospheric CH_4 burden, *Geophys. Res. Lett.*, *36*, L18803, doi:10.1029/2009GL039780.

461

462 Dunkerton, T. J., and D. P. Delisi (1985), The subtropical mesospheric jet observed by the
463 Nimbus 7 limb infrared monitor of the stratosphere, *J. Geophys. Res., 90*, 10,681-10,692.

464

465 Garcia, R. R., D. R. Marsh, D. E. Kinnison, B. A. Boville, and F. Sassi (2007), Simulation of
466 secular trends in the middle atmosphere, 1950-2003, *J. Geophys. Res., 112*, D09301,
467 doi:10.1029/2006JD007485.

468

469 Garcia, R. R., T. J. Dunkerton, R. S. Lieberman, and R. A. Vincent (1997), Climatology of the
470 semiannual oscillation of the tropical middle atmosphere, *J. Geophys. Res., 102*, 26,019-26,032.

471

472 Garcia, R. R., S. Solomon, R. G. Roble, and D. W. Rusch (1984), A numerical response of the
473 middle atmosphere to the 11-year solar cycle, *Planet. Space Sci., 32*, 411-423.

474

475 Gordley, L., E. Thompson, M. McHugh, E. Remsberg, J. Russell III, and B. Magill (2009),
476 Accuracy of atmospheric trends inferred from the Halogen Occultation Experiment data, *J. Appl.*
477 *Remote Sens., 3*, doi:10.1117/1.313722.

478

479 Harries, J. E., et al. (1996), Validation of water vapor from the Halogen Occultation Experiment
480 (HALOE), *J. Geophys. Res., 101*, 10,205-10,216.

Hervig, M., and D. Siskind (2006), Decadal and inter-hemispheric variability in polar mesospheric clouds, water vapor, and temperature, *J. Atmos. Solar-Terr. Phys.*, *68*, 30-41, doi:10.1016/j.jastp.2005.08.010.

Huang, T. Y. W., and G. P. Brasseur (1993), Effect of long-term solar variability in a two-dimensional interactive model of the middle atmosphere, *J. Geophys. Res.*, *98*, 20,413-20,427.

Jackson, D. R., M. D. Burrage, J. E. Harries, L. J. Gray, and J. M. Russell III (1998), The semi-annual oscillation in upper stratospheric and mesospheric water vapour as observed by HALOE, *Q. J. R. Meteorol. Soc.*, *124*, 2493-2515.

Kley, D., J. M. Russell III, and C. Phillips, Eds. (2000), SPARC assessment of upper tropospheric and stratospheric water vapour, *World Climate Research Program (WCRP) Report No. 113*, World Meteorological Organization (WMO) Tech. Doc. #1043, 312 pp.

Lambert, A., et al. (2007), Validation of the Aura Microwave Limb Sounder middle atmosphere water vapor and nitrous oxide measurements, *J. Geophys. Res.*, *112*, D24S36, doi:1029/2007JD008724.

Laštovička, J., et al. (2008), Emerging pattern of global change in the upper atmosphere and ionosphere, *Ann. Geophys., 26,* 1255-1268.

Lossow, S., J. Urban, J. Gumbel, P. Eriksson, and D. Murtagh (2008), Observations of the mesospheric semi-annual oscillation (MSAO) in water vapour by Odin/SMR, *Atmos. Chem. Phys., 8,* 6527-6540.

Luebken, F.-J., U. Berger, and C. Baumgarten (2009), Stratospheric and solar cycle effects on long term variability of mesospheric ice clouds, *J. Geophys. Res.,* doi:10.1029/2009JD012377*, in press.*

Marsh, D. R., R. R. Garcia, D. E. Kinnison, B. A. Boville, F. Sassi, S. C. Solomon, and K. Matthes (2007), Modeling the whole atmosphere response to solar cycle changes in radiative and geomagnetic forcing, *J. Geophys. Res., 112,* D23306, doi:10.1029/2006JD008306.

Marsh, D., A. Smith, and E. Noble (2003), Mesospheric ozone response to changes in water vapor, *J. Geophys. Res., 108*, D3, 4109, doi:10.1029/2002JD002705.

519 McHugh, M., M. Hervig, B. Magill, E. Thompson, E. Remsberg, J. Wrotny, and J. M. Russell III
520 (2003), Improved mesospheric temperature, water vapor, and polar mesospheric cloud
521 extinctions from HALOE, *Geophys. Res. Lett., 30,* doi:10.1029/2002GL016859.

522

523 Milz, M., et al. (2009), Validation of water vapour profiles (version 13) retrieved by the
524 IMK/IAA scientific retrieval processor based on full resolution spectra measured by MIPAS on
525 board Envisat, *Atmos. Meas. Tech., 2,* 379-399.

526

527 Nedoluha, G. E., R. M. Gomez, B. C. Hicks, J. E. Wrotny, C. Boone, and A. Lambert (2009),
528 Water vapor measurements in the mesosphere from Mauna Loa over solar cycle 23, *J. Geophys.*
529 *Res.,* doi:10.1029/2009JD012504, *in press*.

530

531 Randel, W. J., F. Wu, H. Voemel, G. E. Nedoluha, and P. Forster (2006), Decreases in
532 stratospheric water vapor after 2001: links to changes in the tropical tropopause and the Brewer-
533 Dobson circulation, *J. Geophys. Res., 111,* D12312, doi:10.1029/2005JD006744.

534

535 Randel, W. J., F. Wu, J. M. Russell III, J. M. Zawodny, and J. Nash (2000), Interannual changes
536 in stratospheric constituents and global circulation derived from satellite data, in Atmospheric
537 Science Across the Stratopause, 271-285, *Geophysical Monograph 123*, American Geophysical
538 Union, Washington, D. C.

539

540 Remsberg, E. (2008a), On the response of Halogen Occultation Experiment (HALOE)
541 stratospheric ozone and temperature to the 11-year solar cycle forcing, *J. Geophys. Res.*, *113*,
542 D22304, doi:10.1029/2008JD010189.

543

544 Remsberg, E. (2008b), On the observed changes in upper stratospheric and mesospheric
545 temperatures from UARS HALOE, *Ann. Geophys.*, *26*, 1287-1297.

546

547 Remsberg, E. E. (2007), A reanalysis for the seasonal and longer-period cycles and the trends in
548 middle-atmosphere temperature from the Halogen Occultation Experiment, *J. Geophys. Res.*,
549 *112*, D09118, doi:10.1029/2006JD007489.

550

551 Rohs, S., C. Schiller, M. Riese, A. Engel, U. Schmidt, T. Wetter, I. Levin, T. Nakazawa, and S.
552 Aoki (2006), Long-term changes of methane and hydrogen in the stratosphere in the period
553 1978-2003 and their impact on the abundance of stratospheric water vapor, *J. Geophys. Res.*,
554 *111*, D14315, doi:10.1029/2005JD006877.

555

556 Russell, J. M. III, et al. (1993), The halogen occultation experiment, *J. Geophys. Res.*, *98*,
557 10,777-10,797.

Sato, K., S. Watanabe, Y. Kawatani, Y. Tomikawa, K. Miyazaki, and M. Takahashi (2009), On the origin of mesospheric gravity waves, *Geophys. Res. Lett., 36*, doi:10.1029/2009GL039908.

Scherer, M., H. Voemel, S. Fueglistaler, S. J. Oltmans, and J. Staehelin (2008), Trends and variability of Midlatitude stratospheric water vapour deduced from the re-evaluated Boulder balloon series and HALOE, *Atmos. Chem. Phys., 8,* 1391-1402.

Schmidt, H., et al. (2006), The HAMMONIA chemistry climate model: sensitivity of the mesopause region to the 11-year solar cycle and CO_2 doubling, *J. Climate, 19*, 3903-3931.

Shepherd, T. G. (2007), Transport in the middle atmosphere, *J. Meteorol. Soc. Japan, 58B*, 165-191.

Shettle, E. P., M. T. Deland, G. E. Thomas, and J. J. Olivero (2009), Long term variations in the frequency of polar mesospheric clouds in the northern hemisphere from SBUV, *Geophys. Res. Lett., 36,* L02803, doi:10.1029/2008GL036048.

576 Siskind, D. E., M. H. Stevens, and C. R. Englert (2005), A model study of global variability in
577 mesospheric cloudiness, *J. Atmos. Solar-Terr. Phys., 67*, 501-513.

578

579 Sonnemann, G. R., and M. Grygalashvyly (2005), Solar influence on mesospheric water vapor
580 with impact on NLCs, *J. Atmos. Solar-Terr. Phys., 67*, 177-190.

581

582 Tiao, G. C., G. C. Reinsel, D. Xu, J. H. Pedrick, X. Zhu, A. J. Miller, J. J. DeLuisi, C. L. Mateer,
583 and D. J. Wuebbles (1990), Effects of autocorrelation and temporal sampling schemes on
584 estimates of trend and spatial correlation, *J. Geophys. Res., 95*(D12), 20,507-20,517.

585

586 Tobiska, W. K., W. R. Pryor, and J. M. Ajello (1997), Solar hydrogen Lyman-α variation during
587 solar cycles 21 and 22, *Geophys. Res. Lett., 24,* 1123-1126.

588

589 Tsutsui, J., K. Nishizawa, and F. Sassi (2009), Response of the middle atmosphere to the 11-year
590 solar cycle simulated with the Whole Atmosphere Community Climate Model, *J. Geophys. Res.,*
591 *114*, D02111, doi:10.1029/2008JD010316.

592

593 Wallace, J. M., R. L. Panetta, and J. Estberg (1993), Representation of the equatorial
594 stratospheric quasi-biennial oscillation in EOF phase space, *J. Atmos. Sci, 50*, 1751-1762.

595

596 Wrotny, J. E., and J. M. Russell III (2006), Interhemispheric differences in polar mesospheric
597 clouds observed by the HALOE instrument, *J. Atmos. Solar-Terr. Phys., 68*, 1352-1369.

598

599 Table 1—Phase of Maximum of First SAO Cycle (in days since Jan 1)

600

P(hPa)	45S	35	25	15	5	5	15	25	35	45N
0.01	5	8	10	15	32	21	20	20	14	8
0.015	6	5	6	23	38	39	39	32	11	8
0.02	10	6	181	60	71	69	72	66	6	6
0.03	13	10	180	95	98	96	95	107	171	3
0.05	24	20	12	111	115	114	113	144	122	1
0.07	29	27	20	150	127	141	119	144	165	5
0.10	39	33	26	171	140	148	143	111	8	13
0.15	47	37	14	173	160	159	147	111	27	8
0.20	58	39	5	172	171	11	157	172	20	11

601

602

603 Table 2—Phase of Maximum of Annual Cycle (in days since Jan 1)

604

P(hPa)	45S	35	25	15	5	5	15	25	35	45N
0.01	3	3	362	4	145	157	170	180	186	185
0.015	10	10	2	27	120	142	167	186	193	194
0.02	11	14	11	40	117	141	173	195	200	199
0.03	12	16	29	54	131	157	187	204	207	204
0.05	16	21	49	104	173	182	200	213	214	211
0.07	17	21	34	115	185	187	199	217	218	216
0.10	15	23	27	80	175	183	201	221	224	224
0.15	20	22	10	43	167	165	179	221	234	224
0.20	21	21	6	362	185	166	160	206	231	231

605

606

Figure 1. Time series of bin-averaged HALOE SS (solid) and SR (open) H_2O values at 35N and 0.015 hPa (near 75 km). The oscillating curve is the MLR model fit to those values.

Figure 2. Time series of the data minus model H_2O residuals (in ppmv) of Figure 1.

Figure 3. Pressure versus latitude contour plot of the 14-yr, annual average H_2O mixing ratio (in ppmv). Contour interval is 0.4 ppmv and altitude coordinate is approximate.

Figure 4. As in Figure 3, but for the amplitudes of the semi-annual (SAO) terms as a percentage of the 14-yr average values. Contour interval is 5%.

Figure 5. As in Figure 3, but for the amplitudes of the annual (AO) terms as a percentage of the 14-yr average values. Contour interval is 5%.

Figure 6. As in Figure 1, but for 15N and 0.05 hPa.

Figure 7. As in Figure 3, but for the amplitudes of the quasi-biennial (QBO) terms as a percentage of the 14-yr average values. Contour interval is 0.5%.

Figure 8. As in Figure 3, but for the 11-yr "max minus min" responses, as a percentage of the 14-yr average values. Contour values are negative and their interval is 2%.

Figure 9. Time of the maximum of the 11-yr term for H_2O (in years past January 1991 or 2002). The dashed curve denotes 5.5 years (or July 1996), and the contour interval is 0.2 years.

Figure 10. As in Figure 8, but for the solar cycle (or SC-like) "max minus min" H_2O responses as a percentage of the 14-yr average values. Contour interval is 2%.

Figure 11. Pressure versus latitude plot of the linear trends for H_2O in terms of their percentage changes per decade. The zero contour is dashed, and the contour interval is 1.5%/decade.

Figure 12. As in Figure 1, but for 35N and 0.05 hPa.

Figure 13. Pressure versus latitude plot of the temperature amplitudes for the annual cycle (in K). Contour interval is 2 K.

Figure 14. As in Figure 13, but for the 14-yr, annual average temperatures (in K). Contour interval is 5 K.

644

645 **Figure 15.** As in Figure 13, but for the solar cycle (or SC-like), max minus min, temperatures

646 (in K). The negative and zero contours are dashed, and the interval is 0.5 K.

647

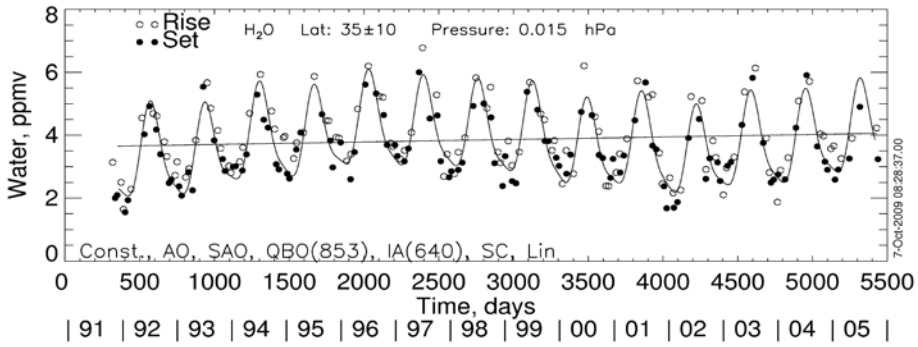

Figure 1. Time series of bin-averaged HALOE SS (solid) and SR (open) H_2O values at 35N and 0.015 hPa (near 75 km). The oscillating curve is the MLR model fit to those values.

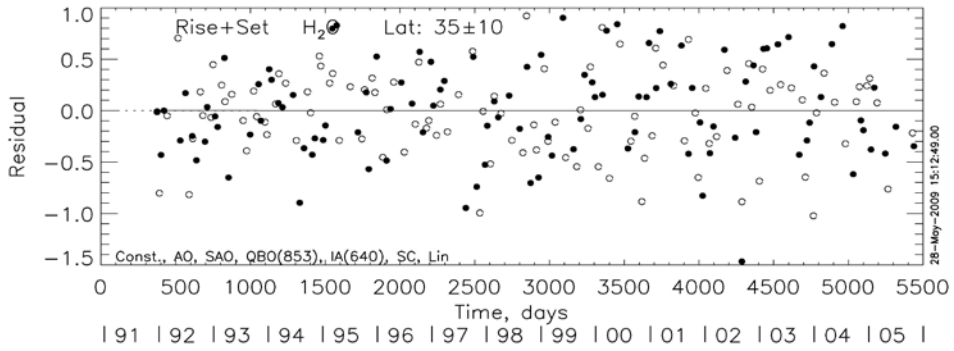

651

652 **Figure 2.** Time series of the data minus model H_2O residuals (in ppmv) of Figure 1.

653

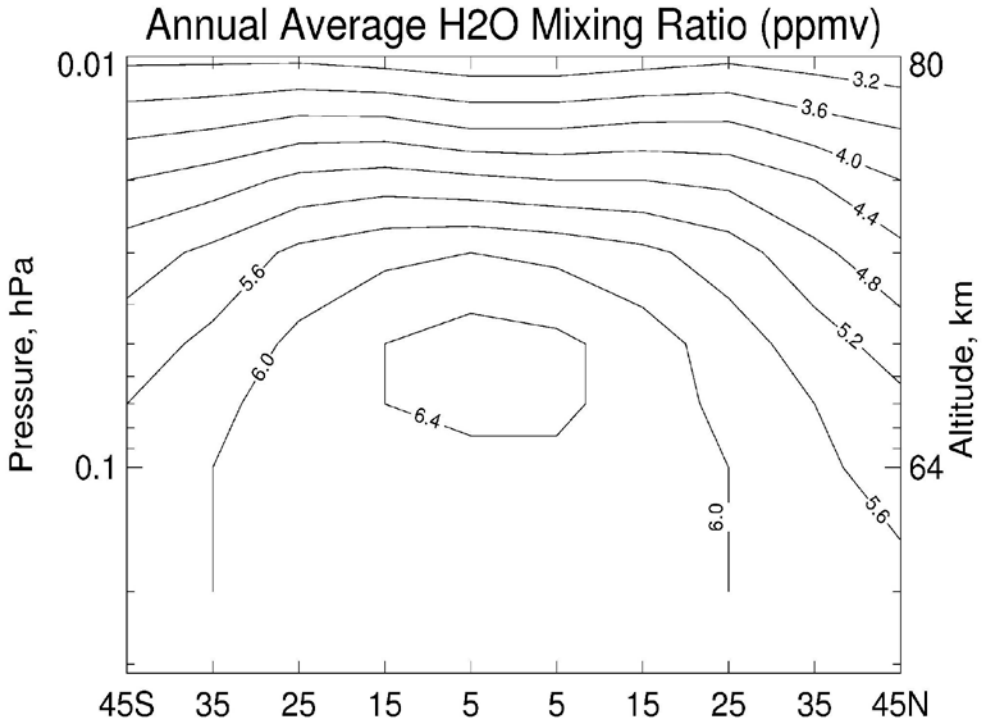

654

655 **Figure 3.** Pressure versus latitude contour plot of the 14-yr, annual average H_2O mixing ratio (in
656 ppmv). Contour interval is 0.4 ppmv and altitude coordinate is approximate.

657

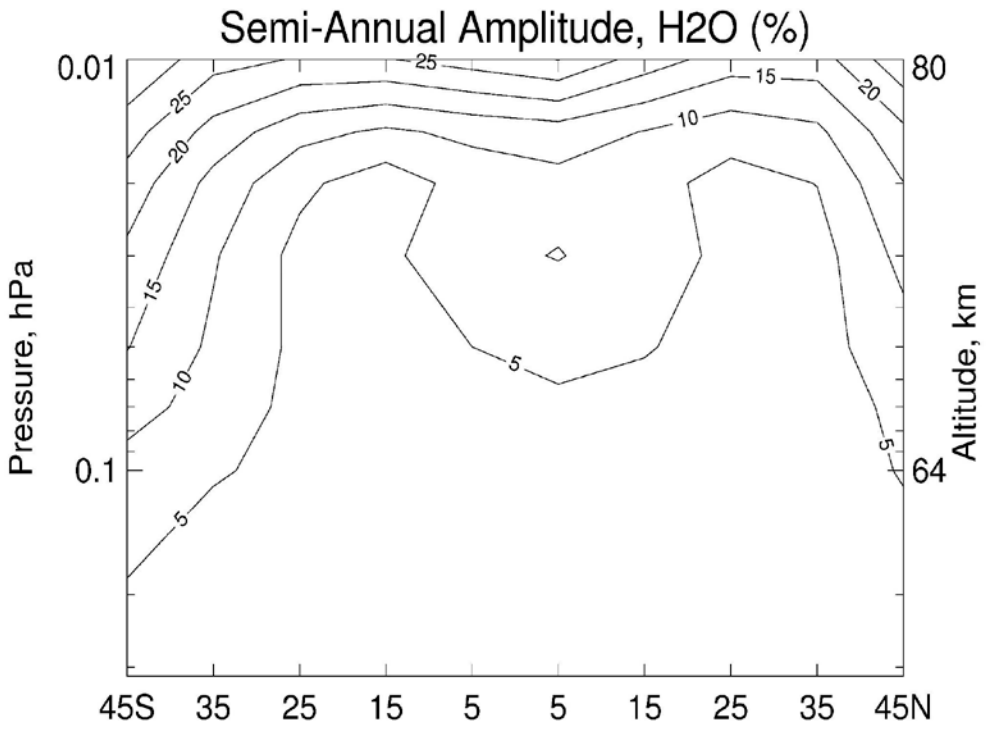

Figure 4. As in Figure 3, but for the amplitudes of the semi-annual (SAO) terms as a percentage of the 14-yr average values. Contour interval is 5%.

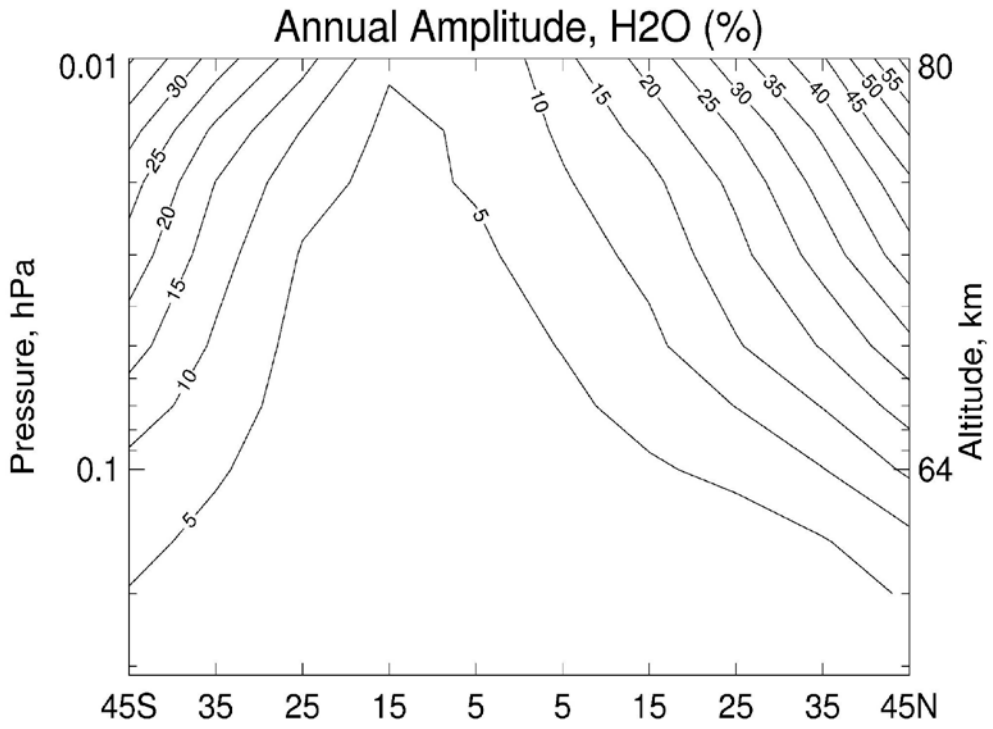

Figure 5. As in Figure 3, but for the amplitudes of the annual (AO) terms as a percentage of the 14-yr average values. Contour interval is 5%.

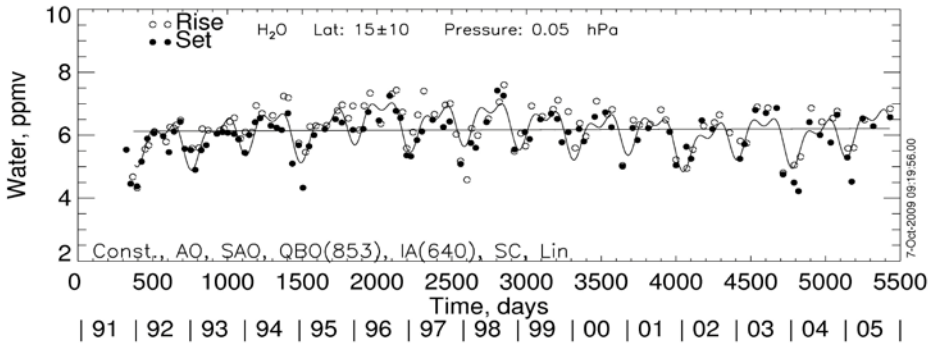

667

668 **Figure 6.** As in Figure 1, but for 15N and 0.05 hPa.

669

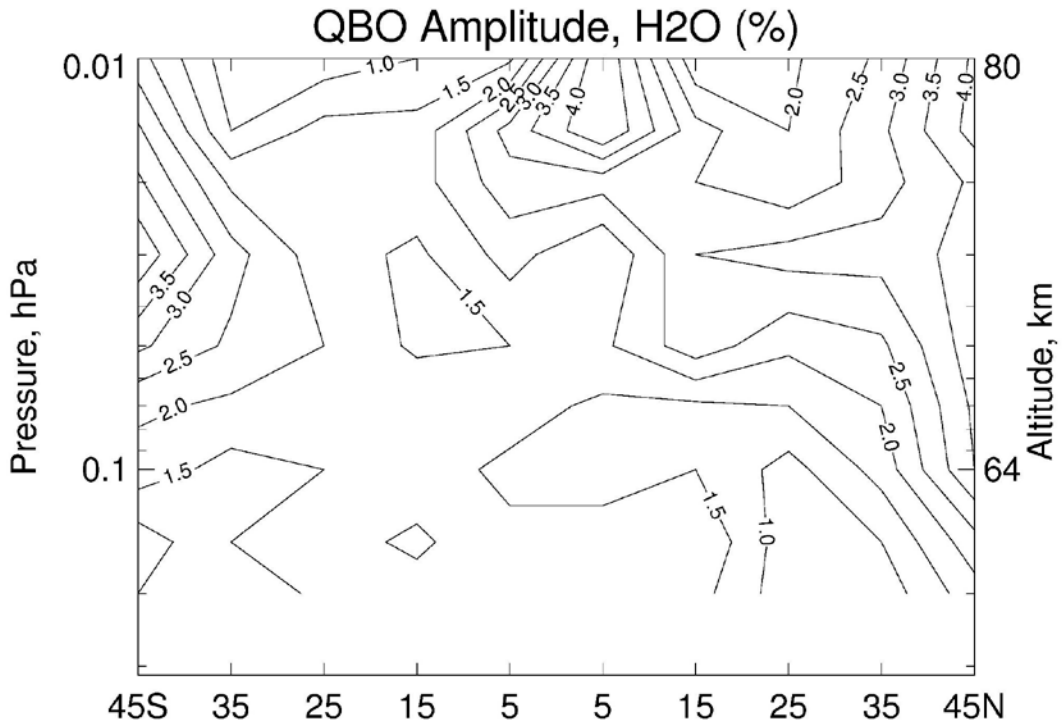

Figure 7. As in Figure 3, but for the amplitudes of the quasi-biennial (QBO) terms as a percentage of the 14-yr average values. Contour interval is 0.5%.

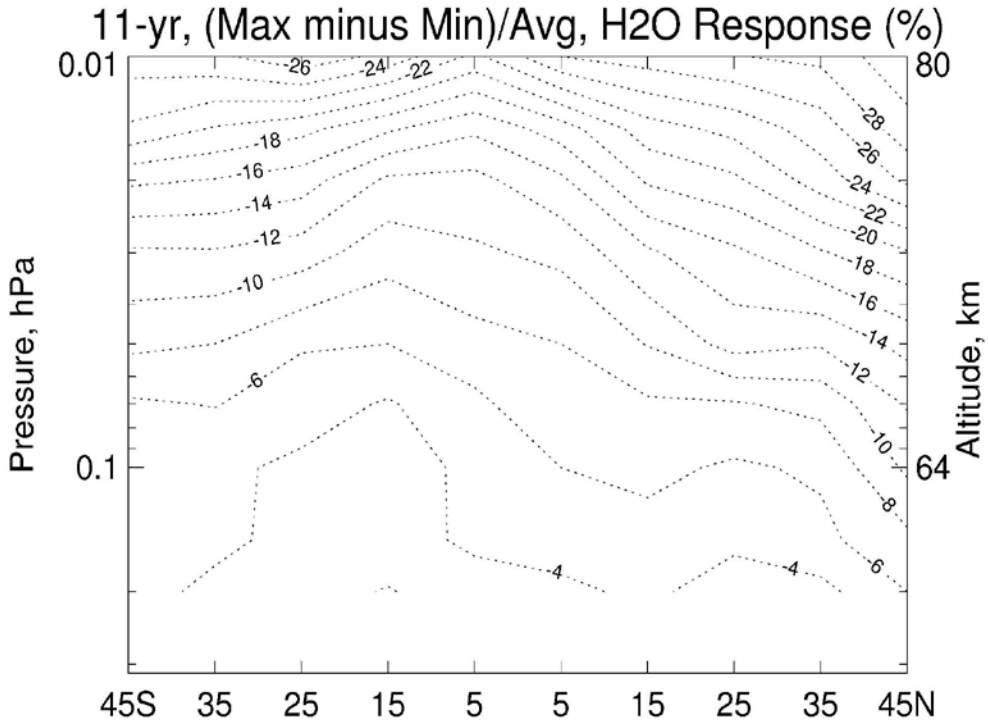

673

674 **Figure 8.** As in Figure 3, but for the 11-yr "max minus min" responses, as a percentage of the
675 14-yr average values. Contour values are negative and their interval is 2%.

676

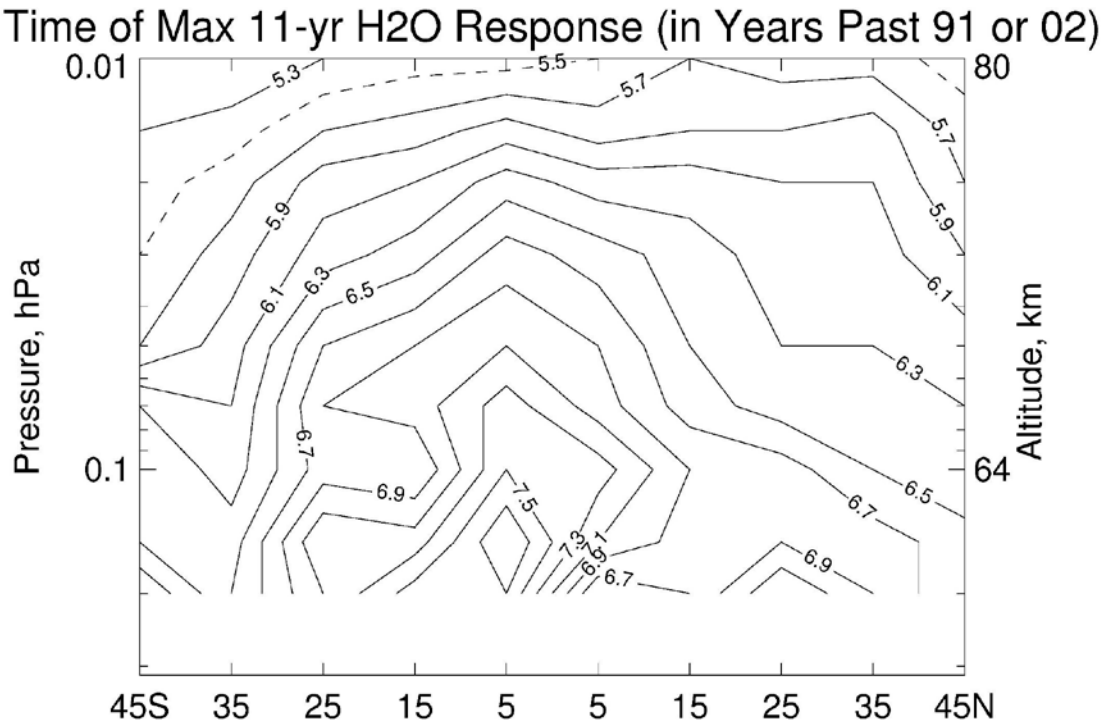

677

678 **Figure 9.** Time of the maximum of the 11-yr term for H_2O (in years past January 1991 or 2002).
679 The dashed curve denotes 5.5 years (or July 1996), and the contour interval is 0.2 years.

680

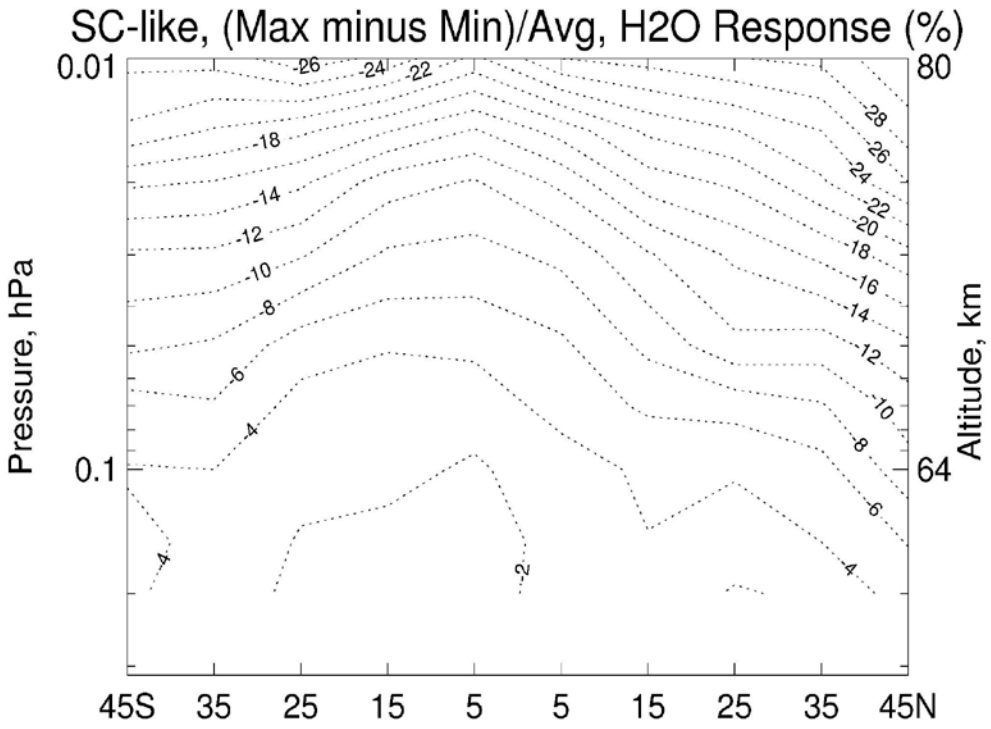

Figure 10. As in Figure 8, but for the solar cycle (or SC-like) "max minus min" H_2O responses as a percentage of the 14-yr average values. Contour interval is 2%.

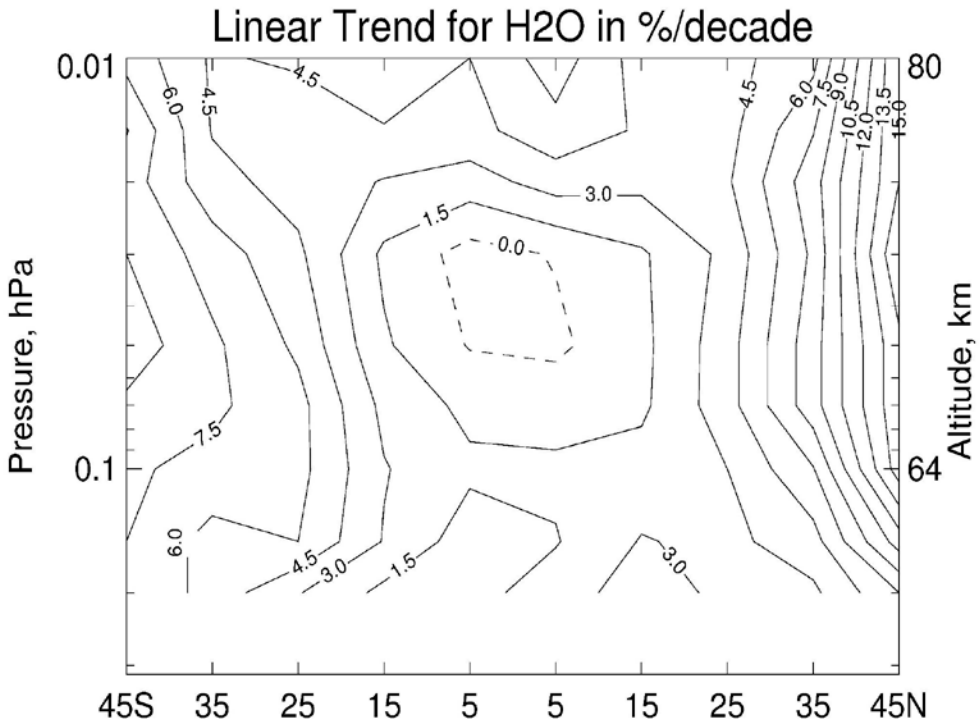

Figure 11. Pressure versus latitude plot of the linear trends for H_2O in terms of their percentage changes per decade. The zero contour is dashed, and the contour interval is 1.5%/decade.

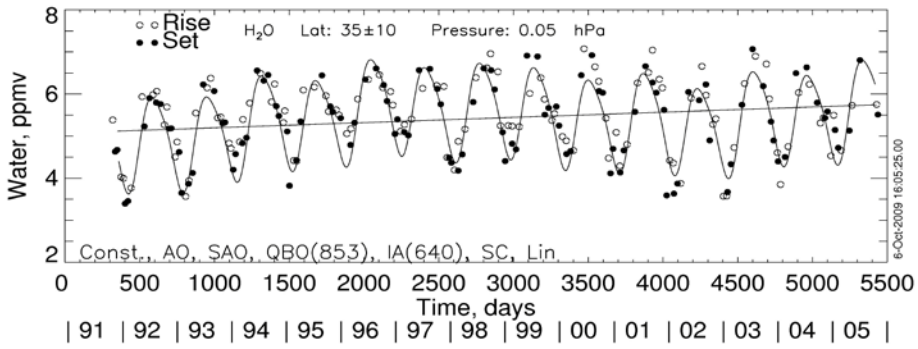

690

691 **Figure 12.** As in Figure 1, but for 35N and 0.05 hPa.

692

693

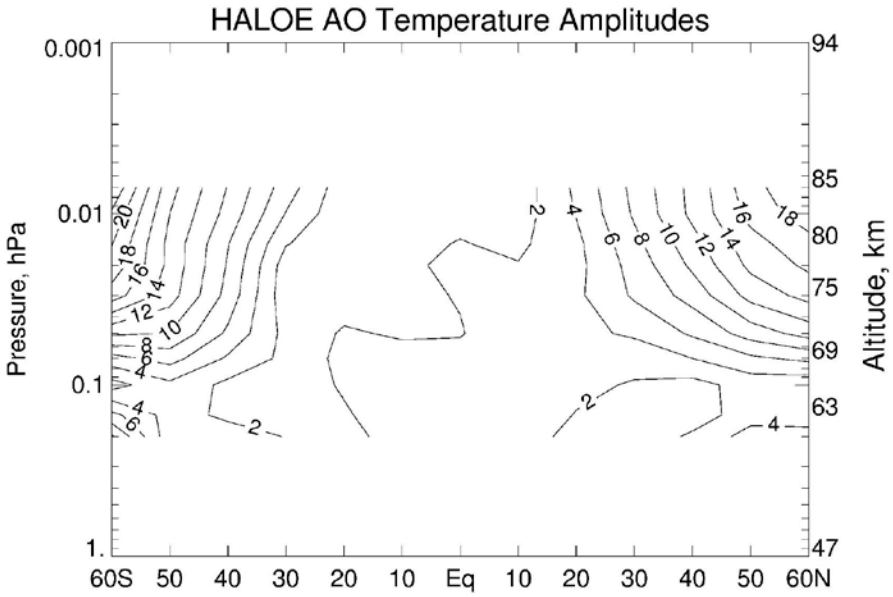

694

695 **Figure 13.** Pressure versus latitude plot of the temperature amplitudes for the annual cycle (in
696 K). Contour interval is 2 K.

697

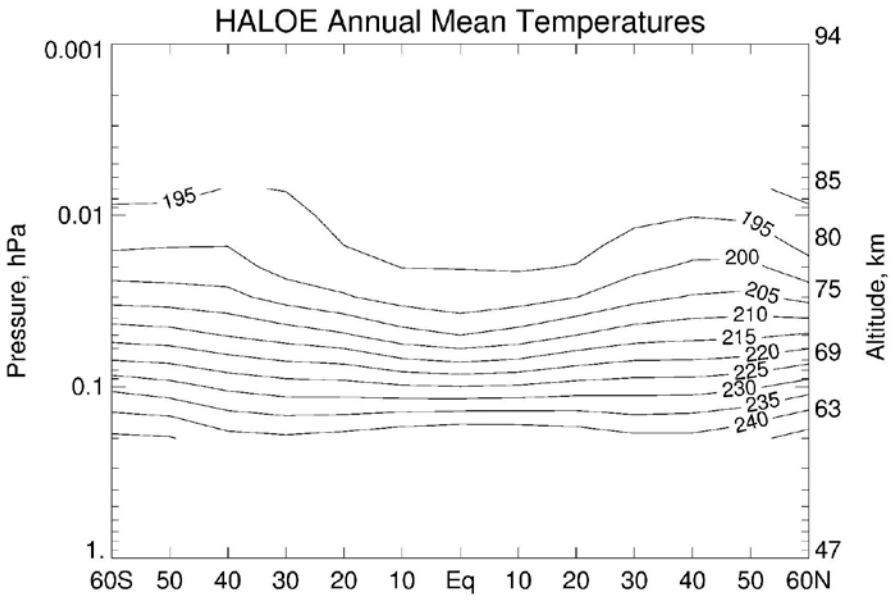

698

699 **Figure 14.** As in Figure 13, but for the 14-yr, annual average temperatures (in K). Contour
700 interval is 5 K.

701

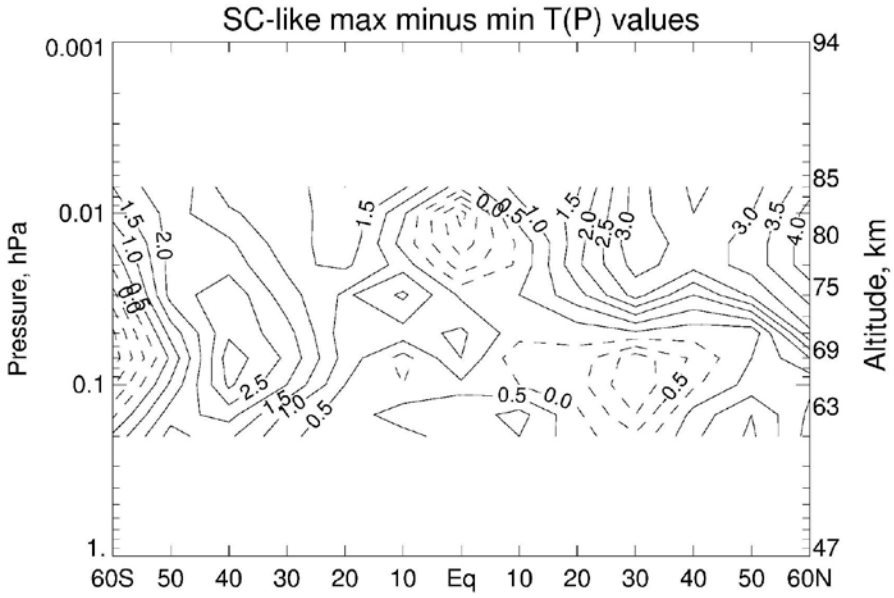

Figure 15. As in Figure 13, but for the solar cycle (or SC-like), max minus min, temperatures (in K). The negative and zero contours are dashed, and the interval is 0.5 K.